

## Article

# Alterations of a CaCl<sub>2</sub> Alginate Composite for Thermochemical Heat Storage during the Hydration in a 1 L Packed Bed Laboratory Reactor

Stephan Heitmann <sup>1,\*</sup>, Tamás Simon <sup>2</sup>, Andrea Osburg <sup>1</sup>  and Michael Fröba <sup>2</sup>

- <sup>1</sup> F. A. Finger-Institute for Building Material Engineering, Chair of Construction Chemistry and Polymer Materials, Bauhaus-Universität Weimar, Coudraystraße 11A, 99423 Weimar, Germany; andrea.osburg@uni-weimar.de
- <sup>2</sup> Department of Chemistry, Institute of Inorganic and Applied Chemistry, University of Hamburg, Martin-Luther-King-Platz 6, 20146 Hamburg, Germany; tamas.simon@uni-hamburg.de (T.S.); michael.froeba@uni-hamburg.de (M.F.)
- \* Correspondence: stephan.lukas.heitmann@uni-weimar.de

**Abstract:** A composite material of alginate and CaCl<sub>2</sub> was tested in a laboratory reactor (1 L) for its ability to thermochemically store heat. The material was exposed to air at 25 °C and 25% RH to prevent the salt from dissolving, and the heat evolution was observed over a period of 15 cycles. To evaluate the changes in the material, samples were taken after 5, 10 and 15 cycles and the material properties and calorimetric characteristics were examined. A change of the material in favor of the heat release was determined, so that an increase of the heat storage capacity from 1.28 kJ·cm<sup>-3</sup> to 2.11 kJ·cm<sup>-3</sup> was detected, with a simultaneous steep decrease of the pore volume in the range from 0.01 to 10 μm. The temperature lift of the reactor showed a significant increase, with the first cycle showing the smallest amount.

**Keywords:** thermochemical heat storage; seasonal storage; calcium chloride; hydration; pore size distribution; cycle stability; reactor experiments



**Citation:** Heitmann, S.; Simon, T.; Osburg, A.; Fröba, M. Alterations of a CaCl<sub>2</sub> Alginate Composite for Thermochemical Heat Storage during the Hydration in a 1 L Packed Bed Laboratory Reactor. *Thermo* **2023**, *3*, 593–604. <https://doi.org/10.3390/thermo3040035>

Academic Editors: Johan Jacquemin and George Z. Papageorgiou

Received: 30 August 2023  
Revised: 26 September 2023  
Accepted: 30 September 2023  
Published: 10 October 2023



**Copyright:** © 2023 by the authors. Licensee MDPI, Basel, Switzerland. This article is an open access article distributed under the terms and conditions of the Creative Commons Attribution (CC BY) license (<https://creativecommons.org/licenses/by/4.0/>).

## 1. Introduction

Since 2012, the addition of solar thermal systems has declined worldwide, and this trend did not end until 2020, despite the circumstances surrounding the Corona pandemic. With 640,000 m<sup>2</sup>, the newly installed collector area in 2021 was approximately at the level of the previous year. Despite this trend, due to weather, the heat generation in 2021 from solar thermal systems was 8.4 billion kWh, approximately five percent less than in 2020 (8.9 billion kWh) [1]. To further advance the construction and use of renewable energy, it is essential to develop more effective seasonal thermal energy to take advantage of the discrepancy between the available heat in summer and the required heat in winter [2]. For seasonal heat storage, thermochemical heat stores are of particular interest, as they have much higher theoretical energy storage densities (100–400 kWh/m<sup>3</sup>) than sensible (20–100 kWh/m<sup>3</sup>) and latent heat stores (50–150 kWh/m<sup>3</sup>) and can be stored without losses [3]. In addition to these three forms, there is also purely adsorptive heat storage, using materials such as silica gel, zeolites or activated carbon [4–6]. The storage mechanism here is based on exothermic sorption and endothermic desorption of water on the surface of porous hydrophilic materials. In the case of adsorptive heat storage, the literature is not entirely in agreement; in some cases, it is assigned to thermochemical heat storage, but sometimes it is listed separately [7]. The energy storage densities of these materials can be further increased if these materials are used as porous carrier structures for salts. In addition to the sorption processes mentioned above, energy storage is also based on the absorption and release of water and the associated hydration and dehydration processes of

the salts [8–11]. A large number of salts have already been investigated for their properties for thermochemical energy storage. A salt that has been studied many times is  $\text{MgSO}_4$ , which shows a very high volumetric storage density of  $2.2 \text{ GJ/m}^3$  between  $\text{MgSO}_4 \cdot \text{H}_2\text{O}$  and  $\text{MgSO}_4 \cdot 7\text{H}_2\text{O}$  [12,13]. The generally high possible storage densities are limited by the slow kinetics of the salt. The hydration process can be accelerated by exceeding the deliquescence humidity, but this is a hindrance to its use as a storage material since the salt is washed out of the porous matrix. The combination of  $\text{MgSO}_4$  with  $\text{MgCl}_2$ , which also causes deliquescence and even increases the storage capacity of the storage material, also has an improving effect [14]. Further investigated salts use  $\text{H}_2\text{O}$  as sorbate  $\text{Li}_2\text{SO}_4 \cdot \text{H}_2\text{O}$  ( $0.9 \text{ kJ/cm}^3$ ),  $\text{CuSO}_4 \cdot 5\text{H}_2\text{O}$  ( $2.07 \text{ kJ/cm}^3$ ) [15] and promising salt hydrates  $\text{MgCl}_2 \cdot 6\text{H}_2\text{O}$  ( $2.5 \text{ kJ/cm}^3$ ) [16],  $\text{SrCl}_2 \cdot 6\text{H}_2\text{O}$  ( $2.51 \text{ kJ/cm}^3$ ) [17] and  $\text{CaCl}_2 \cdot 6\text{H}_2\text{O}$  ( $2.70 \text{ kJ/cm}^3$ ) [18]. In the case of  $\text{SrCl}_2$  and  $\text{CaCl}_2$ , all hydrate stages can be achieved at temperatures below  $150 \text{ }^\circ\text{C}$ , which makes these salts interesting for their application in the domestic heating sector. It should be noted that with chlorides, there is the possibility of hydrolysis with the formation of corrosive compounds. Since salts in the form of powders are not very suitable to be used as storage material, there are some investigations to combine the salts with a porous carrier. The already mentioned zeolites or silica gels are a popular carrier because they are already hygroscopic. However, more passive carrier materials, such as activated carbon or vermiculite, have also been investigated as carrier material [19–22]. Another very interesting carrier material is alginate, which can be easily combined with different salts in a bottom-up approach. The salt content and particle size can be easily controlled to form spherical composites that are very suitable for gas–solid reactions. Additionally, a combination of the alginate support structures with graphite in order to exploit the good properties of graphite such as high specific surface area and high thermal conductivity was achieved [23,24]. This work will address the study of a larger scale of the previously reported  $\text{CaCl}_2$ -alginate composites [24] and demonstrate their changes during loading and unloading in a 1 L reactor. The most important aspect to be considered in this work is the prevention of a  $\text{CaCl}_2$  solution formation in order to minimize the agglomeration of the particles and to avoid salt washout. This, in turn, should lead to a higher cycle stability and make the material permanently well-flowable.

## 2. Materials and Methods

### 2.1. Chemicals

The salts used were obtained from the following manufacturers: Anhydrous granular calcium chloride (Grüssing, Filsum, Germany; 10233U) and sodium alginate (AppliChem, Darmstadt, Germany; A3249,0250).

### 2.2. Preparation of the Calcium Chloride Alginate Composite

For the  $\text{CaCl}_2$  composite, a homogeneous mixture of water (3.2 L) and sodium alginate (64 g) was added dropwise to an aqueous solution of calcium chloride (4.64 kg  $\text{CaCl}_2$  and 6.4 L water) via a funnel with a tap. The aqueous  $\text{CaCl}_2$  solution was filtered for purification prior to the dropping procedure (filter: Macherey-Nagel, MN615  $\frac{1}{4}$ ,  $\text{Ø} = 320 \text{ mm}$ , REF 531 032). During the dropping process (gravity, rt, 250 rpm), agglomeration of the calcium alginate beads was prevented by stirring the salt solution and locating the droplet site outside the stirring vortex. The  $\text{CaCl}_2$  alginate beads were left covered in the salt solution for 24 h, decanted and filtrated, washed with 1.25 L water four times and finally dried via a two-step procedure: (1) rotary evaporation ( $90 \text{ }^\circ\text{C}$ , 150 mbar) for 2 h; (2) storage in an oven for 30 h at  $140 \text{ }^\circ\text{C}$ . An average of 135 to 160 g of calcium alginate beads per batch was obtained via this synthesis process. Figure 1 shows a graphical summary of the synthesis pathway and the processes involved.

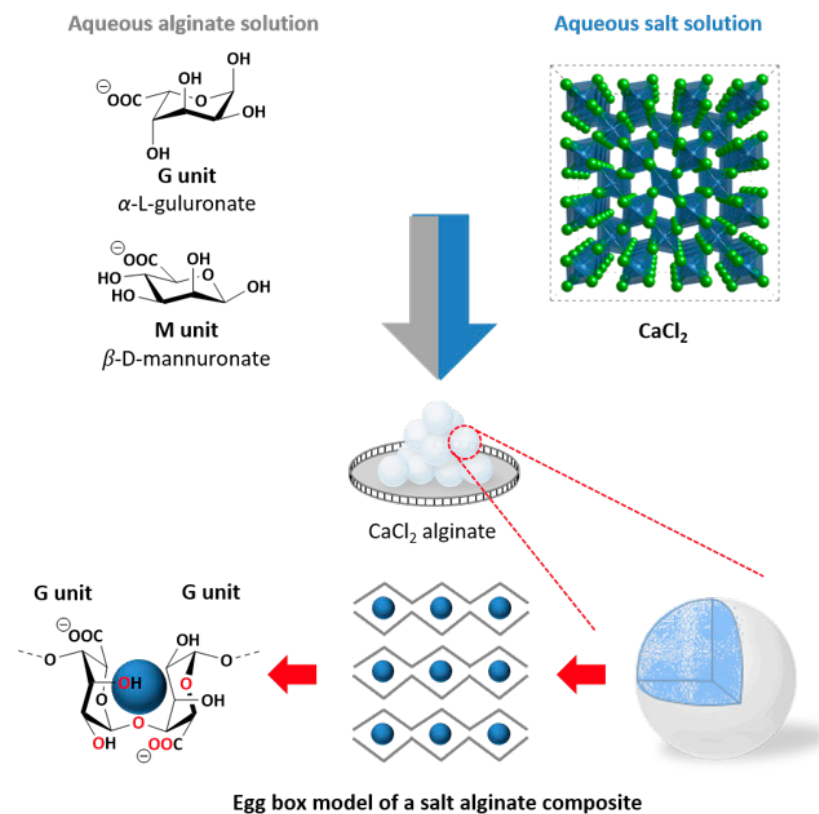


**Figure 1.** Illustration of the synthesis pathway used for the  $\text{CaCl}_2$  alginate composites. The white beads represent the  $\text{CaCl}_2$  alginate composites, and the blue beads represent the  $\text{Ca}^{2+}$  cations responsible for cross-linking the alginate matrix. Egg box model: coordination of the  $\text{Ca}^{2+}$  cations by the atoms marked in red.

### 2.3. Characterization of the Material

The chloride content of the composite material was determined by ion chromatography (IC) on an aqueous eluate. From this, conclusions have then been made regarding the salt content of the storage material. The porosity  $\phi$  of the materials used is determined according to the relationship between bulk density  $\rho$  and pure density  $\rho_0$ , expressed in Equation (1).

$$\phi = \rho / \rho_0, \quad (1)$$

The pure density was determined using a helium pycnometer of the type “AccuPyc 1330” from “Micromeritics” according to the DIN 66137-2 standard [25]. For this purpose, the storage material was dried at 130 °C for 24 h, finely ground, dried again at 130 °C for 24 h, and measured. The bulk density is determined by means of a geopycnometer of the type “Geopyk 1360” from the company “Micromeritics”. In this method, the bulk density is determined by displacing a solid medium, dry flow. This medium formed a dense packing around the object to be examined without penetrating into the pore spaces. By means of nitrogen adsorption, the specific surface area was determined by the Brunauer, Emmett and Teller (BET) method in a “SA 3100” from the company “Coulter” according to the DIN ISO 9277:2014-01 standard [26]. In addition, investigations in an “Autopore IV” mercury porosimeter from “Micromeritics” provided data on pore size distribution, porosity, surface area and mean pore diameter using the ISO 15901-1:2019-03 standard [27]. The storage material was dried in a drying oven at 130 °C for 24 h prior to each test. All IC, pycnometry, MIP and nitrogen adsorption measurements were performed in triplicate. Scanning electron microscope (SEM) images were taken of the raw material as well as after 5, 10 and 15 cycles on a “Hitachi TM3000, Bruker EDX” of some of the particles to visualize possible changes.

#### 2.4. Calorimetric Investigations

The heat release generated by the reaction of the material with water was recorded in a “C80” calorimeter combined with a wet air generator “Wetsys” from “Setaram Instrumentation”. For this purpose, the samples (approximately 50 mg) were heated to a temperature of 130 °C (at 2 K/min) in a reaction cell, while the chamber was purged with a constant volume flow (50 mL/min) of dry nitrogen. At this temperature, the sample can dehydrate well; it can be easily reached with solar thermal systems, and the alginate matrix can withstand it without any problems [24,28]. After a holding time of 2 h, the temperature was lowered to 25 °C at 0.22 K/min; the volume flow of nitrogen remained unchanged. After reaching 25 °C and setting a constant heat flux, the relative humidity was abruptly increased to 20 and 30% RH, respectively. This range between the transition calcium chloride tetrahydrate ( $\text{CaCl}_2 \cdot 4\text{H}_2\text{O}$ )/hexahydrate ( $\text{CaCl}_2 \cdot 6\text{H}_2\text{O}$ ) and the deliquescence line of calcium chloride hexahydrate should ensure that the formation of calcium chloride hexahydrate occurs and no washing out due to solution formation appears [24,29]. Integrating the curve of the heat flux when the material is loaded provides the total heat released from the reaction, i.e., the heat of hydration.

#### 2.5. Thermogravimetry

To determine the amount of water absorbed, the samples were dehydrated in a thermogravimetry following the calorimetry. Previous studies on dehydration of similar composites have shown that  $\text{CaCl}_2 \cdot 2\text{H}_2\text{O}$  can be found at temperatures above 75 °C and  $\text{CaCl}_2$  anhydrate at temperatures above 120 °C [24]. For this purpose, the samples were heated to 130 °C under inert gas and the change in mass was recorded. A simultaneous thermal analysis apparatus “STA 449 F3 Jupiter” from “Netsch” was used.

#### 2.6. Experiments in a 1 L Reactor

To investigate the temperature rise of the material in a reactor bed, a laboratory reactor with a capacity of 1 L was designed and constructed. A sketch of the experimental setup with humid air generation and reactor chamber, as well as sensors for measuring temperature and relative humidity, is shown in Figure 2. This is an open-reactor system in which a constant flow of humid air passes through the storage material from below. A cylindrical stainless-steel chamber with a diameter of 101 mm and a height of 155 mm formed the reaction chamber. At the inlet and outlet, the chamber was tapered to 19 mm, which also corresponded to the diameter of the air duct. The storage material was held in place by a stainless-steel mesh screen and the entire system was thermally insulated with a 20 mm fiberglass mat. The humid air was generated by means of two mass flow controllers (MFC), one that controlled dry air and one that controlled the flow of humid air via a bubbler; back pressure valves secured the MFCs. These two air streams were merged, whereupon the humidity and temperature were measured for the first time in a chamber in front of the reactor vessel. This chamber and the area directly below the particle bed were intended to ensure that the airflow was homogeneously mixed and uniform. A second humidity sensor was placed behind the particle bed. The humidity sensors used were “DMTHM8XX” from the company “DM-Sensors”; the temperature sensors in the particle bed were common sheathed thermocouples of type K. An amount of 599 g of composite material was examined, which was dehydrated in a drying oven at 130 °C for 24 h prior to performing the experiment. It was then cooled to room temperature in desiccators and afterwards transferred to the reactor chamber. The temperature of the incoming air depended on the ambient conditions and ranged between 20 and 23 °C. The water content of the air used was between 20 and 23% RH at a volume flow of 10 L/min. Temperatures were recorded over a course of 65 h, and a total of fifteen (energetic) discharge cycles were performed and recorded. After the fifth, tenth and fifteenth cycles, a few grams of material were taken in each case to analyze any changes in the material.

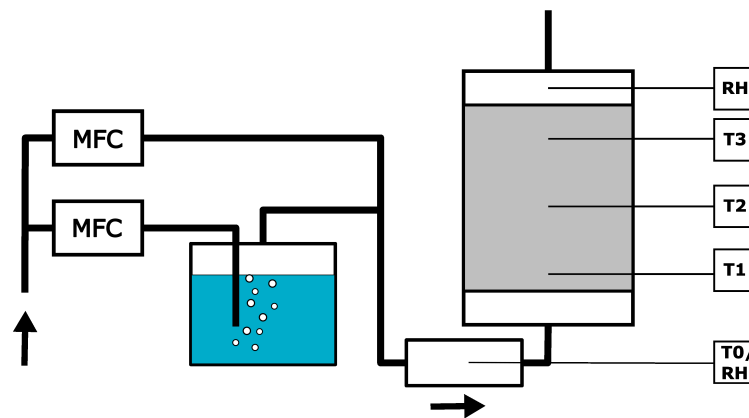


**Figure 2.** Drawing of the experimental setup with the moist air generation on the left and the reactor chamber on the right with four measuring points for temperature (T) and two for relative humidity (RH). The arrow describes the flow direction of the air, and the flow rate is adjusted by two mass flow controllers (MFCs).

### 3. Results and Discussion

#### 3.1. Material Properties

The values determined by ion chromatography, mercury intrusion porosimetry (MIP), nitrogen adsorption and pycnometry are shown in Table 1. The chloride content was determined by ion chromatography at 44.1 wt%, suggesting a maximum  $\text{CaCl}_2$  mass fraction of 69 wt%. The average pore diameter  $d_{av}$ , total porosity  $\phi_{MIP}$  and specific surface area  $S_{MIP}$  were determined via MIP. The bulk density  $\rho$  was determined via a geopycnometer and the pure density  $\rho_0$  via helium adsorption. The determined bulk density of the MIP with  $0.96 \text{ g/cm}^3$  confirms the determined value of  $\rho_0$ . The calculated total porosity  $\phi_{cal}$  of 53% was compared with the open porosity of the MIP  $\phi_{MIP}$  of 28%. This resulted in a closed porosity of 25% in a pore range  $> 6 \text{ nm}$ . The value of the specific surface area, which was determined by the BET method from the isotherms of the nitrogen sorption, is not meaningful, since the isotherm suggests that the proportion of micro- and mesopores is extremely low. Figure 3 shows the adsorption and desorption isotherms of nitrogen adsorption of the untreated  $\text{CaCl}_2$  alginate particles. This assumption is confirmed by MIP measurements, shown in Figure 4 top left, where 79% of the samples were determined to be macroporous. Therefore, the value of the specific surface area determined by MIP seems to be more accurate, despite the assumption of a cylindrical mantle surface [30,31]. In addition, Figure 4 also shows the pore size distribution determined by MIP after cycles five, ten and fifteen.

**Table 1.** Material properties of the composite determined by ion chromatography (weight percentage of calcium chloride  $w_{\text{CaCl}_2}$ ), pycnometry (pure density  $\rho_0$ , bulk density  $\rho$ ), nitrogen adsorption (specific surface area  $S_{BET}$ ) and MIP (bulk density  $\rho_{MIP}$ , porosity  $\phi_{MIP}$ , specific surface area  $S_{MIP}$ , average pore diameter  $d_{av}$ ). The porosity  $\phi_{cal}$  was calculated using Equation (1).

Cycle	$w_{\text{CaCl}_2}$ (wt%)	$\rho_0$ ( $\text{g/cm}^3$ )	$\rho$ ( $\text{g/cm}^3$ )	$\rho_{MIP}$ ( $\text{g/cm}^3$ )	$\phi_{MIP}$ (%)	$\phi_{cal}$ (%)	$S_{BET}$ ( $\text{m}^2/\text{g}$ )	$S_{MIP}$ ( $\text{m}^2/\text{g}$ )	$d_{av}$ (nm)
raw	69.0	2.00	0.97	0.96	28	53	1.4	36	61
5	-	-	0.86	0.84	14	57	1.1	17	60
10	-	-	1.21	1.52	14	40	1.0	15	43
15	-	-	1.09	1.57	10	45	1.0	8	52

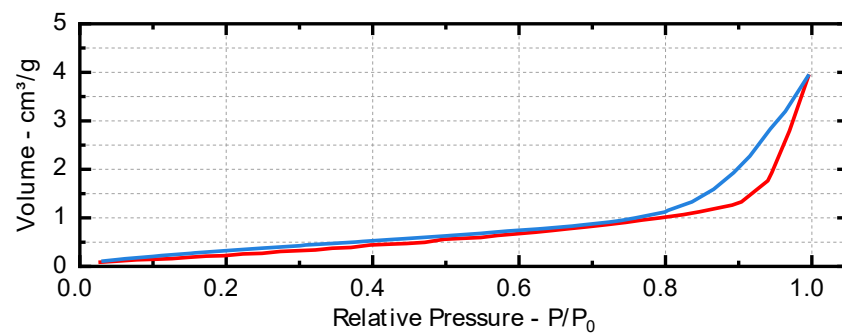


**Figure 3.** Adsorption (red) and desorption (blue) isotherm of nitrogen adsorption of the uncyclized material.

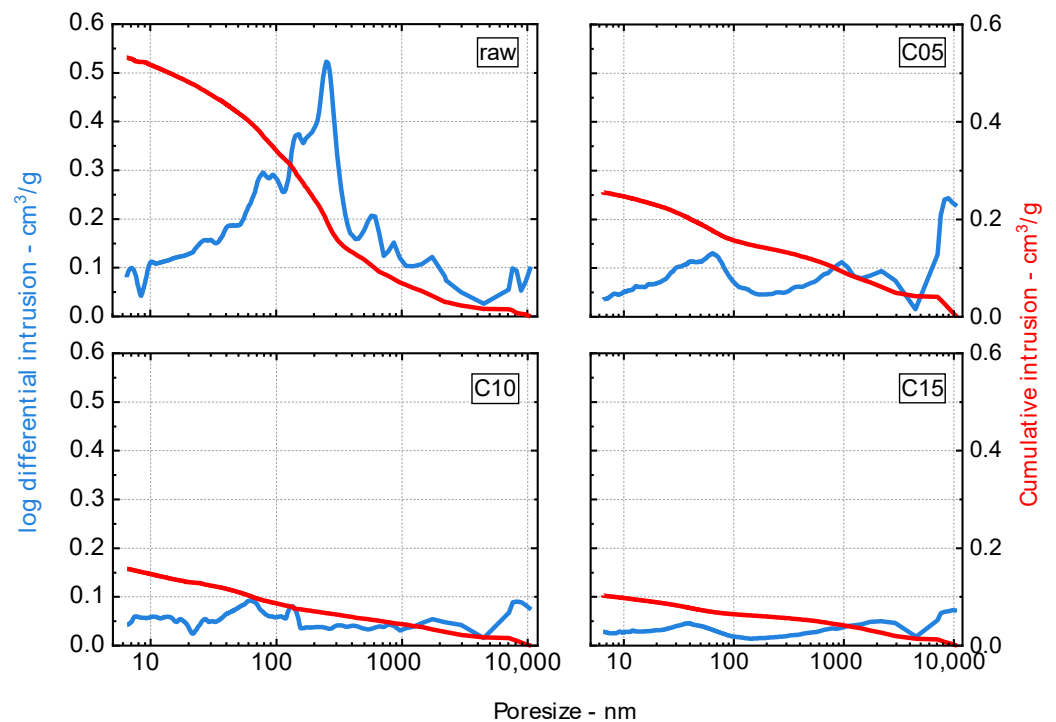


**Figure 4.** Mercury intrusion porosimetry of the raw storage material and after 5, 10 and 15 cycles. The log differential intrusion is the blue line; the cumulative intrusion is the red line.

Evaluations of MIP over the course of 15 cycles show a very strong decrease in the pores in all size ranges. After five cycles, for example, it can be observed that the large proportion of pores in the 250 nm range has disappeared, and a far more homogeneous distribution of pore sizes has occurred. Looking at the next ten cycles, a much less significant decrease in pore size is observed, but the total volume of pores has decreased from  $0.53 \text{ cm}^3/\text{g}$  to  $0.1 \text{ cm}^3/\text{g}$ . As a result, the densities determined no longer conform to the raw densities determined by pycnometry. In this case, the density of the MIP is considered inaccurate since the calculation basis for the density is also lost as a result of the disappearance of the pore space, and this also applies to the specific surface area and porosity values. This disappearance of pores can be attributed to the density and concomitant volume change from non-hydrated  $\text{CaCl}_2$  to calcium chloride hexa- and tetrahydrate ( $\text{CaCl}_2 \cdot 6\text{H}_2\text{O}$ ;  $\text{CaCl}_2 \cdot 4\text{H}_2\text{O}$ ) as well as solution formation [18]. Images taken with the scanning electron microscope illustrate this in Figure 5. Here, the growing crack structures are clearly visible, which can be attributed to the expansion during water absorption and contraction during drying. In combination with these crack formations, density changes that peak after the 10th cycle at  $\rho = 1.21$  and result in a porosity change to  $\phi_{\text{cal}} = 40\%$  can be observed. After 15 cycles, these values decrease to  $\rho = 1.09$ , resulting in a porosity of  $\phi_{\text{cal}} = 45\%$ .

Accompanied by this, a decrease in the specific surface area can be observed. The effects of the changing material parameters can be seen above all in the following subsections.

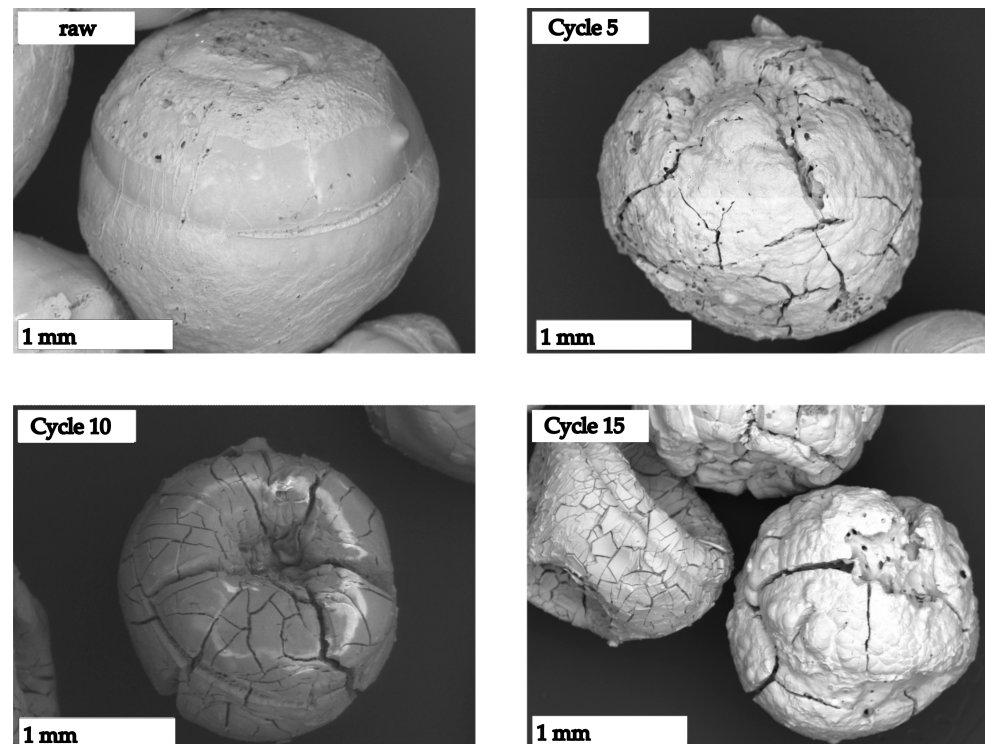


**Figure 5.** SEM images of representative particles of the raw material and after 5, 10 and 15 cycles passed.

### 3.2. Calorimetry

The key feature of a heat storage material, the energy storage density, is determined by calorimetric investigations. The results are presented in Table 2 along with the literature values. The determined values refer to the consideration of the materials as a packed bed, as indicated by the authors. The material used is similar to that of Kallenberger except for the salt content, which in his case is between 80 and 90 wt%; in contrast, the value determined for the material studied here is 69 wt%. The salt contents of Kallenberger refer to the lowest available hydrate grade, and the salt content of this work refers to pure salt. To ensure the optimal energy yield and an almost compact material, it is desirable to reach the hydrate stage of  $\text{CaCl}_2 \cdot 6\text{H}_2\text{O}$  without any formation of solution. This requires safe handling of temperature and humidity since the melting temperature of hexahydrate is about 25 °C at humidities of about 30% RH [32]. The selected parameters of 25 °C and 20% RH are intended to ensure that the optimum energy yield is achieved without solution formation [29,32,33]. The determined storage densities of the raw material of 1.28 kJ/cm<sup>3</sup> and 1.39 kJ/cm<sup>3</sup> are in the range of those of a similar composite material reported by the literature at 1.50 kJ/cm<sup>3</sup> and 1.10 kJ/cm<sup>3</sup> [24] and exceed those of storage materials with vermiculite as carrier with 1.2 kJ/cm<sup>3</sup> [22]. Although, in the reported material there was dissolution or no formation of the  $\text{CaCl}_2$  hexahydrate [22,24]. As the number of cycles increases and the material parameters change, in particular porosity and density, an increase in the heat of hydration can be detected. Especially in the experiments with a humidity of 30% RH, an increase of up to 0.84 kJ/cm<sup>3</sup> has been analyzed, same as the values of the experiments with lower humidity which also show an increase in hydration heat. In combination with the density changes of the material, the energy storage density thus also increases to its maximum at 2.11 kJ/cm<sup>3</sup> at 25 °C and 20% RH and 2.23 kJ/cm<sup>3</sup> at 25 °C and 30% RH after the fifteenth cycle.

**Table 2.** Results of the calorimetric and thermogravimetric investigations of the raw storage material and after 5, 10 and 15 cycles of hydration and dehydration. The storage densities are calculated with the density  $\rho$  and the measured heat of reaction. The water absorption refers to the dry storage material.

	Temperature [°C]/ Relative Humidity [%]	Heat of Reaction [kJ/kg]	Storage Density [kJ/cm <sup>3</sup> ] ([kWh/m <sup>3</sup> ])	Water Uptake [g <sub>H2O</sub> /g <sub>sample dry</sub> ]
CCA-raw	25/20	1324	1.28 (357)	0.35
	25/30	1478	1.39 (387)	0.64
CCA-C05	25/20	1343	1.13 (313)	0.39
	25/30	1790	1.50 (418)	0.61
CCA-C10	25/20	1036	1.57 (437)	0.33
	25/30	1271	1.93 (537)	0.32
CCA-C15	25/20	1347	2.11 (587)	0.47
	25/30	1419	2.23 (619)	0.48
CCA-K [24]	30/20	1018	1.10 (306)	0.64
	30/30	1206	1.50 (417)	0.88

### 3.3. Thermogravimetry

The samples loaded in the calorimeter were promptly examined thermogravimetrically after the measurement to determine the amount of water absorbed. The amount of water absorbed during loading can be used to draw conclusions about the hydrate levels in the composite. Thermogravimetric analysis of the material loaded at 25 °C and 20% RH showed a mass loss of 24% and thus a water content of 0.35 g<sub>H2O</sub>/g<sub>sample dry</sub>. Assuming that the salt was not hydrated at the beginning of the experiment, this amount would not be enough to completely convert the salt present into the hexahydrate. Thus, it must be assumed that only part of the salt participated in the reaction. Looking at later cycles, it is noticeable that with a slight increase in water uptake, significantly more heat energy is released, so that after 15 cycles the water uptake has increased to 0.47 g<sub>H2O</sub>/sample dry while the heat yield increased considerably from 1.28 to 2.11 kJ/cm<sup>3</sup>. This increase in water adsorption is due to the formation of cracks and the “opening” of the pores, which were discussed in Section 3.1. When looking at the material loaded at 30% RH, it is noticeable that the water absorption decreases from 0.64 to 0.48 g<sub>H2O</sub>/sample dry (after 10 cycles even to 0.32 g<sub>H2O</sub>/sample dry). This may be related to the disappearance of the small pores; it is possible that part of the water in the raw material is not stored as hydrate water but in capillary pores. Because these account for a smaller and smaller proportion as the number of cycles increases, and at the same time more and more salt becomes accessible via crack formation, a lower or similar water absorption can lead to increased heat release. The lower water absorption compared to the literature value specimens may be due to the lower salt content, the other test parameters of temperature and humidity or a possibly different pore pattern. Exact statements on this cannot be made due to the lack of material parameters.

### 3.4. Reactor Experiments

The temperature gradients of the reactor tests after one, five, ten and fifteen cycles are shown in Figure 6, as are the differences in relative humidity between the inlet and outlet of the reactor chamber. When observing the first cycle, a small temperature deviation of 3 K can be seen, which increases over the period of ten cycles to a maximum of 6.5 K. In addition to the increase in the temperature deviation, a broadening of the temperature peak can be observed, i.e., a higher temperature yield with a constant amount of air fed in. From the tenth cycle on, a decrease in the temperature peak can be observed, which has decreased down to 5 K after the fifteenth cycle. The temperature and humidities of the incoming air were between 20 to 23 °C and 20 to 23% RH, respectively. The humidity difference between the incoming and outgoing air was 6% RH at the end of the experiment, indicating that loading was not yet complete at this point. Furthermore, from the difference in the water content of the air, it can be concluded that the uncycled material can absorb

much less water than the storage materials of later cycles, which is finally evident in the increasing temperature yield. In addition to the amount of water absorbed, the reaction rate, i.e., the kinetics of the material, also increases as the number of cycles increases. These two findings are supported by the material properties collected and can be attributed to the “opening” of the pores and the rupturing of the particles, respectively. This leads to the water in the air reaching the salt inside more easily, thus hydrating it further to broaden and increase the temperature peaks, which eventually leads to a higher heat yield. For one application, this would mean an almost threefold temperature output over the course of 12 h, dropping to the value of 2 K in the following 12 h. Under these conditions, the maximum temperature swing is nevertheless a good 50% below the 12 to 21 K already reported [24] and a further 30% lower than the latest findings for alginate/graphite- $\text{CaCl}_2$  composites [23]. In the latter, it was also taken into account that the salt goes into the solution. Although fusion of the particles was observed, no significant drawbacks were found during the five cycles. To achieve these temperatures with the material studied in this work, it would have to be accepted that the deliquescence line would be exceeded. In direct comparison with tested zeolite storage tanks, which operated at 40 to 60% RH, it is noticeable that the temperature range is also much lower here, although the  $\text{CaCl}_2$  alginates compounds operate at only one-third of the humidity [34,35].

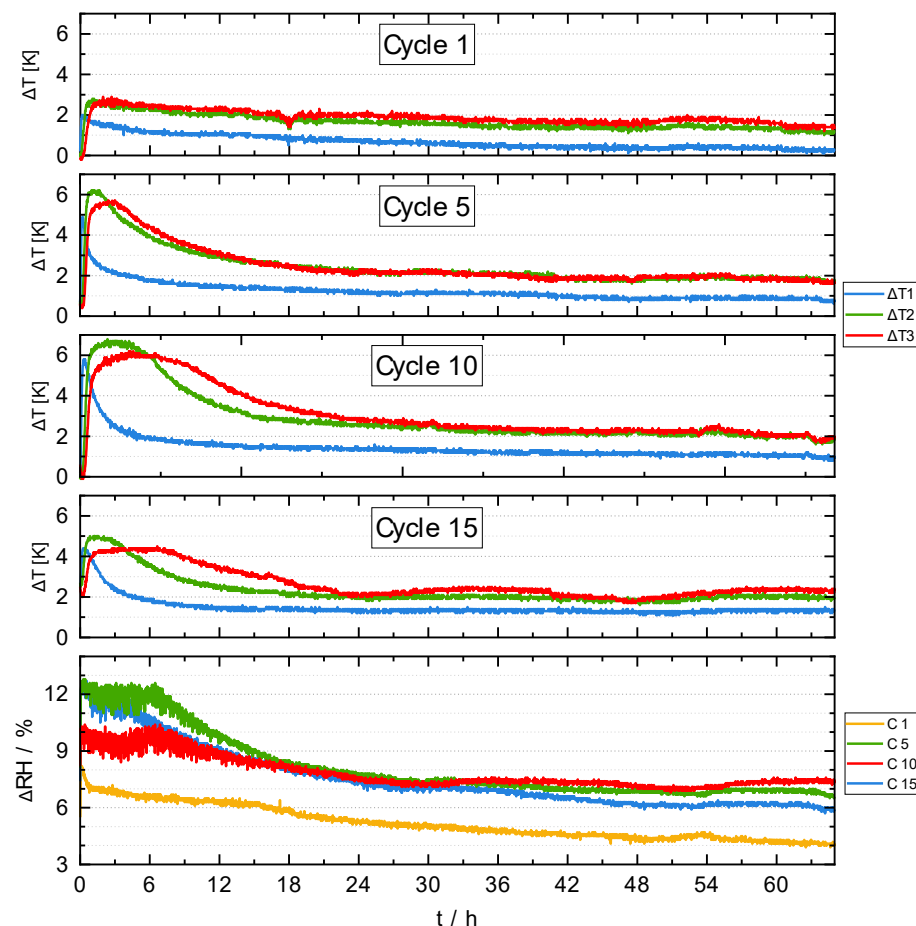


**Figure 6.** Temperature lift of a laboratory reactor filled with 599 g  $\text{CaCl}_2$ -alginate particles. The temperature lift is represented by three temperature differences from the bottom ( $\Delta T1$ ) to the top ( $\Delta T3$ ). In addition, the differences in humidity between incoming and outgoing air are shown. The temperatures of the tests were between 20 and 23 °C, and the humidity values were between 20 and 23% RH.

#### 4. Conclusions

Large amounts of a  $\text{CaCl}_2$  alginate composite for thermochemical heat storage were studied in a 1 L reactor. The temperature developments in this particle bed were studied over 15 cycles, and the changes in the material were detected. The material values around porosity, pore distribution, densities, energy storage density and water absorption were collected from the raw material as well as after five, ten and fifteen cycles. Explicit care was taken to avoid dissolution of the salt hydrate to avoid agglomeration and washing out of the salt.

An amount of 599 g of a  $\text{CaCl}_2$  composite material embedded in an alginate matrix with a salt content of 69 wt% was loaded into a cylindrical reactor chamber with humid air (20 to 23% RH; 20 to 23 °C) at a flow rate of 10 L/min. The temperature evolution during the reaction inside the reactor chamber as well as the changing porosities, densities, water absorption and heat of the reaction between cycles were determined. During loading, care was taken not to exceed the deliquescence moisture content of the  $\text{CaCl}_2 \cdot 6\text{H}_2\text{O}$  as well as  $\text{CaCl}_2 \cdot 4\text{H}_2\text{O}$ .

The untreated material had an open porosity of 28%, with 79% of the pores being macropores. The total volume of the pores decreased from  $0.53 \text{ cm}^3/\text{g}$  to  $0.1 \text{ cm}^3/\text{g}$  over 15 cycles and severe crack growth was observed on the particles, with no apparent loss of stability. This cracking goes along with an increase of the bulk density up to 1.09, a decrease of the porosity to 45% and a decrease of the specific surface area. However, as the cracking seems to lead to better accessibility of the salt inside the particles, the water absorption increases from  $0.35 \text{ g}_{\text{H}_2\text{O}}/\text{g}_{\text{sample dry}}$  to  $0.47 \text{ g}_{\text{H}_2\text{O}}/\text{g}_{\text{sample dry}}$  and results in higher energy storage densities of the composite. These energy storage densities were detected over the course of the cycles, and an increase from  $1.28 \text{ kJ}/\text{cm}^3$  ( $357 \text{ kWh}/\text{m}^3$ ) to  $2.11 \text{ kJ}/\text{cm}^3$  ( $587 \text{ kWh}/\text{m}^3$ ) could be determined. With further approximation and probable exceeding of the deliquescence moisture, even higher energy storage densities of  $1.39 \text{ kJ}/\text{cm}^3$  ( $387 \text{ kWh}/\text{m}^3$ ) up to  $2.23 \text{ kJ}/\text{cm}^3$  ( $619 \text{ kWh}/\text{m}^3$ ) could be obtained. In contrast to this, in some cases, a higher energy yield with lower water absorption of the storage material was analyzed. A possible explanation for this may be the storage of water in capillary pores, the number of which decreases after a few cycles. This issue needs to be examined in more detail. The simultaneous formation of cracks may mean that salt is easier to reach in the interior.

The investigations show that the storage material by no means exhibits stable properties over 15 cycles but that the energy storage density actually improves over the course of a few cycles. The mechanical stability is not strongly influenced by the investigated cycles. The number of cycles for mechanical stability to be influenced remains to be clarified, but other work in this area reports more than 100 cycles of the same material. The temperature lift is and remains small and further confirms the complications of seasonal heat storage based on  $\text{CaCl}_2$ . However, the increase in heat storage capacity and, in particular, the sharply increasing temperature output as the number of cycles increases may be of interest to other salt-hydrate storage systems.

**Supplementary Materials:** The following supporting information can be downloaded at: <https://www.mdpi.com/article/10.3390/thermo3040035/s1>, calorimetric and thermogravimetric measurements of the calcium chloride alginate composite particles.

**Author Contributions:** Conceptualization, S.H.; methodology, S.H. and T.S.; validation, S.H.; formal analysis, S.H.; investigation, S.H.; resources, A.O.; data curation, S.H.; writing—original draft preparation, S.H. and T.S.; writing—review and editing, A.O. and M.F.; visualization, S.H. and T.S.; supervision, A.O.; project administration, A.O. and M.F.; funding acquisition, A.O. and M.F. All authors have read and agreed to the published version of the manuscript.

**Funding:** This research was funded by the BMBF (Bundesministerium für Bildung und Forschung), as part of the project AlgiTherm with the project number 03EK3060A-B.

**Data Availability Statement:** The data presented in this study are available in the present article and in the related Supplementary Materials.

**Acknowledgments:** We are grateful to our project partners from Hamburg, especially Steiger, and Jens Schneider (Bauhaus-Universität Weimar) for the helpful discussions. Furthermore, we acknowledge support for the publication costs by the Open Access Publication Fund of Bauhaus-Universität Weimar. A special thanks goes to our funder, the BMBF, who made the AlgiTherm project (03EK3060A-B) possible in the first place.

**Conflicts of Interest:** The funders had no role in the design of the study; in the collection, analyses, or interpretation of data; in the writing of the manuscript; or in the decision to publish the results.

## Nomenclature

CCA-raw	calcium chloride alginate composite uncycled
CCA-CXX	calcium chloride alginate composite after XX cycles
CCA-K	calcium chloride alginate composite uncycled of literature source [24]
$d_{av}$	average pore diameter
RH	relative humidity
S	specific surface area
T	temperature
t	time
$w_{CaCl_2}$	mass fraction of $CaCl_2$
Greek symbols	
$\rho$	bulk density
$\rho_0$	raw density
$\Phi$	porosity
Subscripts	
0	Raw (0 cycles)
BET	Brunauer-Emmett-Teller
cal	calculated
MIP	mercury intrusion porosimetry

## References

1. Energien-Statistik Arbeitsgruppe Erneuerbare. Erneuerbare Energien in Deutschland Daten zur Entwicklung im Jahr 2021. Available online: <https://www.umweltbundesamt.de/publikationen/erneuerbare-energien-in-deutschland-0> (accessed on 29 September 2023).
2. Imbery, F.; Friedrich, K.; Kaspar, F.; Fleckenstein, R.; Lengefeld, K.; Bissolli, P.; Daßler, J. Klimatologische Einordnung des Jahres 2021. Available online: [https://www.dwd.de/DE/klimaumwelt/aktuelle\\_meldungen/220105/deutschland\\_klimarueckblick\\_2021.html](https://www.dwd.de/DE/klimaumwelt/aktuelle_meldungen/220105/deutschland_klimarueckblick_2021.html) (accessed on 29 September 2023).
3. Rundel, P.; Meyer, B.; Meiller, M.; Meyer, I.; Daschner, R.; Jakuttis, M.; Franke, M.; Binder, S.; Hornung, A. *Studie Speicher fuer die Energiewende*. Sulzbach-Rosenberg, 2013. Available online: [https://www.umsicht-suro.fraunhofer.de/content/dam/umsicht-suro/de/documents/studien/studie\\_speicher\\_energiewende.pdf](https://www.umsicht-suro.fraunhofer.de/content/dam/umsicht-suro/de/documents/studien/studie_speicher_energiewende.pdf) (accessed on 29 September 2023).
4. Mette, B.; Kerskes, H.; Drück, H.; Müller-Steinhagen, H. Experimental and numerical investigations on the water vapor adsorption isotherms and kinetics of binderless zeolite 13X. *Int. J. Heat. Mass. Transf.* **2014**, *71*, 555–561. [CrossRef]
5. Núñez, T.; Mittelbach, W.; Henning, H.-M. Development of an adsorption chiller and heat pump for domestic heating and air-conditioning applications. *Appl. Therm. Eng.* **2007**, *27*, 2205–2212. [CrossRef]
6. Kaneko, K. Micropore filling mechanism in inorganic sorbents. *Stud. Surf. Sci. Catal.* **1996**, *99*, 573–598. [CrossRef]
7. N'Tsoukpoe, K.E.; Liu, H.; Le Pierrès, N.; Luo, L. A review on long-term sorption solar energy storage. *Renew. Sustain. Energy Rev.* **2009**, *13*, 2385–2396. [CrossRef]
8. N'Tsoukpoe, K.E.; Schmidt, T.; Rammelberg, H.U.; Watts, B.A.; Ruck, W.K.L. A systematic multi-step screening of numerous salt hydrates for low temperature thermochemical energy storage. *Appl. Energy* **2014**, *124*, 1–16. [CrossRef]
9. Aristov, Y.I.; Tokarev, M.M.; Cacciola, G.; Restuccia, G. Selective water sorbents for multiple applications, 1.  $CaCl_2$  confined in mesopores of silica gel: Sorption properties. *React. Kinet. Catal. Lett.* **1996**, *59*, 325–333. [CrossRef]
10. Jänchen, J.; Ackermann, D.; Weiler, E.; Stach, H.; Brösicke, W. Calorimetric investigation on zeolites,  $AlPO_4$ 's and  $CaCl_2$  impregnated attapulgite for thermochemical storage of heat. *Thermochim. Acta* **2005**, *434*, 37–41. [CrossRef]
11. Tso, C.Y.; Chao, C.Y.H. Activated carbon, silica-gel and calcium chloride composite adsorbents for energy efficient solar adsorption cooling and dehumidification systems. *Int. J. Refrig.* **2012**, *35*, 1626–1638. [CrossRef]

12. van Essen, V.M.; Zondag, H.A.; Gores, J.C.; Bleijendaal, L.P.J.; Bakker, M.; Schuitema, R.; van Helden, W.G.J.; He, Z.; Rindt, C.C.M. Characterization of  $\text{MgSO}_4$  Hydrate for Thermochemical Seasonal Heat Storage. *J. Sol. Energy Eng.* **2009**, *131*, 4. [CrossRef]
13. Posern, K.; Kaps, C. Humidity controlled calorimetric investigation of the hydration of  $\text{MgSO}_4$  hydrates. *J. Therm. Anal. Calorim.* **2008**, *92*, 905–909. [CrossRef]
14. Posern, K.; Kaps, C. Calorimetric studies of thermochemical heat storage materials based on mixtures of  $\text{MgSO}_4$  and  $\text{MgCl}_2$ . *Thermochim. Acta* **2010**, *502*, 73–76. [CrossRef]
15. Ferchaud, C.J.; Zondag, H.A.; de Boer, R. Material Research on Salt Hydrates for Seasonal Heat Storage Application in a Residential Environment. In Proceedings of the International Symposium on Innovative Materials for Processes in Energy System (IMPRESS 2013), Fukuoka, Japan, 4–6 September 2013.
16. van Essen, V.M.; Cot Gores, J.; Bleijendaal, L.P.J.; Zondag, H.A.; Schuitema, R.; Bakker, M.; van Helden, W.G.J. Characterization of Salt Hydrates for Compact Seasonal Thermochemical Storage. In Proceedings of the ASME 2009 3rd International Conference on Energy Sustainability collocated with the Heat Transfer and InterPACK09 Conferences, San Francisco, CA, USA, 19–23 July 2009; ASME: Houston, TX, USA, 2009; Volume 2, pp. 825–826.
17. Steiger, M. Thermodynamic properties of  $\text{SrCl}_2(\text{aq})$  from 252 K to 524 K and phase equilibria in the  $\text{SrCl}_2\text{--H}_2\text{O}$  system: Implications for thermochemical heat storage. *J. Chem. Thermodyn.* **2018**, *120*, 106–115. [CrossRef]
18. N'Tsoukpoe, K.E.; Rammelberg, H.U.; Lele, A.F.; Korhammer, K.; Watts, B.A.; Schmidt, T.; Ruck, W.K.L. A review on the use of calcium chloride in applied thermal engineering. *Appl. Therm. Eng.* **2015**, *75*, 513–531. [CrossRef]
19. Gordeeva, L.G.; Restuccia, G.; Freni, A.; Aristov, Y.I. Water sorption on composites “LiBr in a porous carbon”. *Fuel Process. Technol.* **2002**, *79*, 225–231. [CrossRef]
20. Simonova, I.A.; Freni, A.; Restuccia, G.; Aristov, Y.I. Water sorption on composite “silica modified by calcium nitrate”. *Microporous Mesoporous Mater.* **2009**, *122*, 223–228. [CrossRef]
21. Gordeeva, L.G.; Tokarev, M.M.; Parmon, V.N.; Aristov, Y.I. Selective water sorbents for multiple application, 6. Freshwater production from the atmosphere. *React. Kinet. Catal. Lett.* **1998**, *65*, 153–159. [CrossRef]
22. Gaeini, M.; Rouws, A.L.; Salari, J.W.O.; Zondag, H.A.; Rindt, C.C.M. Characterization of microencapsulated and impregnated porous host materials based on calcium chloride for thermochemical energy storage. *Appl. Energy* **2018**, *212*, 1165–1177. [CrossRef]
23. Reynolds, J.; Williams, R.; Elvins, J.; Jewell, E.; Searle, J.; Ke, X. Development and characterisation of an alginate and expanded graphite based composite for thermochemical heat storage. *J. Mater. Sci.* **2023**, *58*, 5610–5624. [CrossRef]
24. Kallenberger, P.A.; Posern, K.; Linnow, K.; Brieler, F.J.; Steiger, M.; Fröba, M. Alginate-Derived Salt/Polymer Composites for Thermochemical Heat Storage. *Adv. Sustain. Syst.* **2018**, *2*, 1700160. [CrossRef]
25. DIN 66137-2: 2019-03; Bestimmung der Dichte fester Stoffe\_-Teil\_2: Gaspyknometrie. Beuth Verlag GmbH: Berlin, Germany, 2019.
26. DIN ISO 9277:2014-01; Bestimmung der spezifischen Oberfläche von Festkörpern mittels Gasadsorption\_-BET-Verfahren (ISO\_9277:2010). Beuth Verlag GmbH: Berlin, Germany, 2014.
27. DIN ISO 15901-1: 2019-03; Bewertung der Porengrößenverteilung und Porosität von Feststoffen mittels Quecksilberporosimetrie und Gasadsorption\_- Teil\_1: Quecksilberporosimetrie (ISO\_15901-1:2016). Beuth Verlag GmbH: Berlin, Germany, 2019.
28. Stach, H.; Mugele, J.; Jänchen, J.; Weiler, E. Influence of Cycle Temperatures on the Thermochemical Heat Storage Densities in the Systems Water/Microporous and Water/Mesoporous Adsorbents. *Adsorption* **2005**, *11*, 393–404. [CrossRef]
29. Pátek, J.; Klomfar, J.; Součková, M. Solid–Liquid Equilibrium in the System of  $\text{CaCl}_2\text{--H}_2\text{O}$  with Special Regard to the Transition Points. *J. Chem. Eng. Data* **2008**, *53*, 2260–2271. [CrossRef]
30. Rouquerol, J.; Avnir, D.; Fairbridge, C.W.; Everett, D.H.; Haynes, J.M.; Pernicone, N.; Ramsay, J.D.F.; Sing, K.S.W.; Unger, K.K. Recommendations for the characterization of porous solids (Technical Report). *Pure Appl. Chem.* **1994**, *66*, 1739–1758. [CrossRef]
31. Barrett, E.P.; Joyner, L.G.; Halenda, P.P. The Determination of Pore Volume and Area Distributions in Porous Substances. I. Computations from Nitrogen Isotherms. *J. Am. Chem. Soc.* **1951**, *73*, 373–380. [CrossRef]
32. Simon, T.; Dohrmann, M.; Steiger, M.; Fröba, M. Calcium Chloride Alginate Composites as Thermochemical Heat Storage Media and the Influence of Different Alginate Species on the Behavior of the Composites. *in preparation*.
33. Carlsson, B.; Stymne, H.; Wettermark, G. An incongruent heat-of-fusion system— $\text{CaCl}_2\cdot 6\text{H}_2\text{O}$ —Made congruent through modification of the chemical composition of the system. *Sol. Energy* **1979**, *23*, 343–350. [CrossRef]
34. Kerskes, H.; Mette, B.; Bertsch, F.; Asenbeck, S.; Drück, H. Chemical energy storage using reversible solid/gas-reactions (CWS—Results of the research project. *Energy Procedia* **2012**, *30*, 294–304. [CrossRef]
35. Kerskes, H.; Sommer, K.; Müller-Steinhagen, H.M. Final Report: Integrales Konzept zur solarthermischen Gebäudeheizung mit Sorptionswärmespeicher. *MonoSorp (BWK25006)*. Stuttgart. 2007. Available online: [https://pudi.lubw.de/detailseite/-/publication/77219-Monosorp\\_-\\_Integrales\\_Konzept\\_zur\\_solarthermischen\\_Geb%C3%A4udeheizung\\_mit\\_Sorptionsw%C3%A4rmespeicher.pdf](https://pudi.lubw.de/detailseite/-/publication/77219-Monosorp_-_Integrales_Konzept_zur_solarthermischen_Geb%C3%A4udeheizung_mit_Sorptionsw%C3%A4rmespeicher.pdf) (accessed on 29 August 2023).

**Disclaimer/Publisher’s Note:** The statements, opinions and data contained in all publications are solely those of the individual author(s) and contributor(s) and not of MDPI and/or the editor(s). MDPI and/or the editor(s) disclaim responsibility for any injury to people or property resulting from any ideas, methods, instructions or products referred to in the content.